EasyChair Preprint

№ 3977

Electromechanical Properties of Monolayer Sn-dichalcogenides

Bach Le Xuan, Thanh Vuong Van, Bao Hoang Van,
Do Van Truong and Hung Nguyen Tuan

July 30, 2020

Electromechanical properties of monolayer Sn-dichalcogenides

Le Xuan Bach[1], Vuong Van Thanh[1*], Hoang Van Bao[1], Do Van Truong[2], Nguyen Tuan Hung[3]

[1*]Department of Design of Machinery and Robot, School of Mechanical Engineering,
Hanoi University of Science and Technology, Hanoi, Vietnam
thanh.vuongvan@hust.edu.vn
[2]Department of Mechatronics, School of Mechanical Engineering,
Hanoi University of Science and Technology, Hanoi, Vietnam
[3]Frontier Research Institute for Interdisciplinary Sciences,
Tohoku University, Sendai 980-8578, Japan

Abstract. We investigate electromechanical properties of monolayer SnX_2 (X = Se, Te) with 1T structure as a function of charge (electron and hole) doping by using first-principles calculations. We find that the monolayer $SnSe_2$ shows a semiconductor-metal transition for the case of heavy electron doping, while $SnTe_2$ retains the metallic properties under both electron and hole dopings. The actuation strain of SnX_2 in the case of electron doping is substantially larger than those of hole doping. Moreover, the effect of charge doping on ideal strength and ideal strain of the monolayer SnX_2 is also discussed.

Keywords: Artificial muscles**,** ideal strength, density functional theory.

1. Introduction

Artificial muscles are materials that can respond like a natural muscle to generate strain and force when stimulated [1,2]. Various actuation materials have been examined to replace the natural muscle such as polymer nanofiber films [3], shape-memory alloys [4], ionic-polymer/metal composites [5], dielectric elastomers [6], and carbon nanotube bundles [7]. Recently, two-dimensional (2D) materials show great potential for the artificial muscle because of their outstanding properties such as large surface doping and mechanical flexibility [8-11]. Acerce *et al.* [12] observed that 2D nanosheet MoS_2 generates mechanical stresses of about 17 MPa with a actuation strain ~ 0.8% at a low voltage between -0.3 and 0.3 V. In the previous theoretical study, Thanh *et al.* [13] investigated the electromechanical properties of other 2D MoS_2 family, and indicated that WTe_2 and WS_2 with 1H and 1T structures, respectively, show the best actuation performances among MX_2 (M = Mo, W; X = S, Se, and Te) compounds. Very recently, other 2D material such as monolayer $SnSe_2$ has been synthesized by the chemical vapor deposition method [14, 15]. Qu *et al*. [16] investigated the mechanical and electronic properties of the monolayer SnX_2 based on the first-principles calculations, and pointed out that under strain, semiconductor-metal transition occurs on SnX_2 with the 2H structure, while the change of the bandgap appears in SnX_2 with the 1T structure. Using an electric-double-layer transistor (EDLT) gating geometry, Zeng *et al*. [17] reported the gate-induced 2D superconductivity in layered 1T-$SnSe_2$. Moreover, magnetism of the monolayer SnX_2 (X = S, Se) was studied [18], in which a phase transition from nonmagnetic to ferromagnetic ground state appears once above the critical hole density (~10^{14} cm^{-2}). Up to date, almost studies of the monolayer SnX_2 have mainly focused on synthesis, mechanical, electronic, and magnetism properties [14-18], while their electromechanical properties are still lacking.

In this paper, by using first-principles calculations, we investigate the electromechanical properties of the monolayer SnX_2 (X = Se, Te) with the 1T structure (1T- SnX_2) as a function of electron and hole dopings. We find that the semiconductor-metal transition occurs in 1T-$SnSe_2$ under a heavy electron doping, while 1T-$SnTe_2$ retains metallic properties under charge doping. The

monolayer $SnSe_2$ shows a reversible strain ranging from 0.5% to 1.8%, making them suitable for actuation applications. Moreover, the ideal strength and the ideal strain of the monolayer SnX_2 under the different charge doping are investigated as well in this study.

2. Computational methods

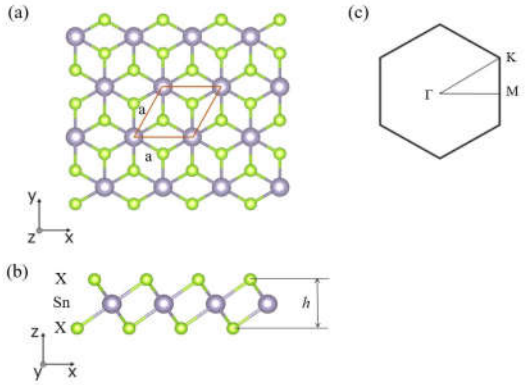

Fig. 1. Top view (a) and front view (b) of monolayer 1T-SnX_2. (c) The first Brillouin zone of monolayer SnX_2 with high-symmetry points.

In this study, we perform the first-principles calculations based on the density-functional theory (DFT) using Quantum ESPRESSO package [19]. The pseudopotentials of Sn, Se and Te from the Standard Solid-State Pseudopotentials library are used [20]. An kinetic energy cut-off for the wave function chosen is 60 Ry. The exchange-correlation energy is evaluated by general gradient approximation using the Perdew–Burke–Ernzerhof (PBE) function [21]. **k**-point grid in the Brillouin zone is set by a 16 × 16 × 1 grid for the monolayer SnX_2 within the Monkhorst–Pack method [22].

The atomic structures of the monolayer SnX_2 is shown in Fig. 1, in which the periodic boundary condition is applied in all models, and a vacuum space of 30 Å in the direction perpendicular to the monolayer (*z*-direction) is set to avoid virtual interactions between layers. To obtain optimized atomic configurations of SnX_2, the atomic positions and cell vectors are relaxed using the Broyden–Fletcher–Goldfarb–Shanno (BFGS) minimization method [23–26] until all the Hellmann–Feynman forces and all components of the stress are less than 0.0005 Ry/a.u. and 0.05 GPa, respectively.

The optimized structured is obtained for each charge doping from -0.1 to +0.1 electron per atom (*e*/atom) to calculate the actuation strain ε^q of the monolayer SnX_2. The electron (hole) doping is simulated by adding (removing) electrons to the unit cell with a uniform charge background [13]. To investigate the ideal strength σ^i (or the maximum stress) and ideal strain ε^i (ε^i is the strain at the maximum stress) of the monolayer SnX_2, an axial tensile strain is applied to the structures by elongating the cell in the axial direction with an increment of 0.02 of the tensile strain until the structure is broken. Here, the dimensionless tensile strain is defined by $\varepsilon = (L - L_0)/L_0$, where L and L_0 are the lengths of the unit cells for strained and unstrained structures, respectively.

3. Results and discussion

Table 1. Lattice constant a_0 (Å), buckling height h (Å), bond lengths of Sn-X and X-X atoms (Å), and $\widehat{XSnX}$ of monolayer SnX_2.

Materials	a	h	Sn-X	X-X	$\widehat{XSnX}$
$SnSe_2$	3.83	3.24	2.74	3.92	91.3^0
$SnTe_2$	4.11	3.60	2.98	4.31	92.7^0

Our calculated lattice constants of the monolayer SnX_2 are listed in Table 1, which are in good agreement with the previous results [27-29], indicating that the present calculations are consistent. The buckling height (h, see Fig. 1(b)) of $SnSe_2$ (3.24 Å) is smaller than that of $SnTe_2$ (3.60 Å) and $MoSe_2$

(3.34 Å) [30]. In addition, our calculations for the Sn-Se and Sn-Te bond lengths are 2.74 Å and 2.98 Å, which are in good agreement with previous DFT calculations [29].

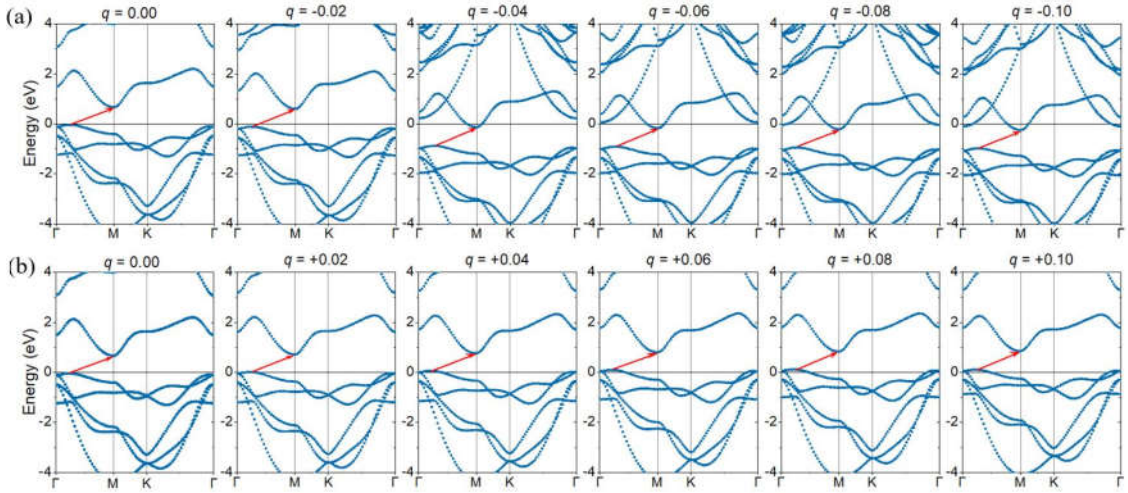

Fig. 2. Energy band structures of monolayer $SnSe_2$ with several (a) electron and (b) hole doping levels. The Fermi energies (dashed line) are set to zero for all plots.

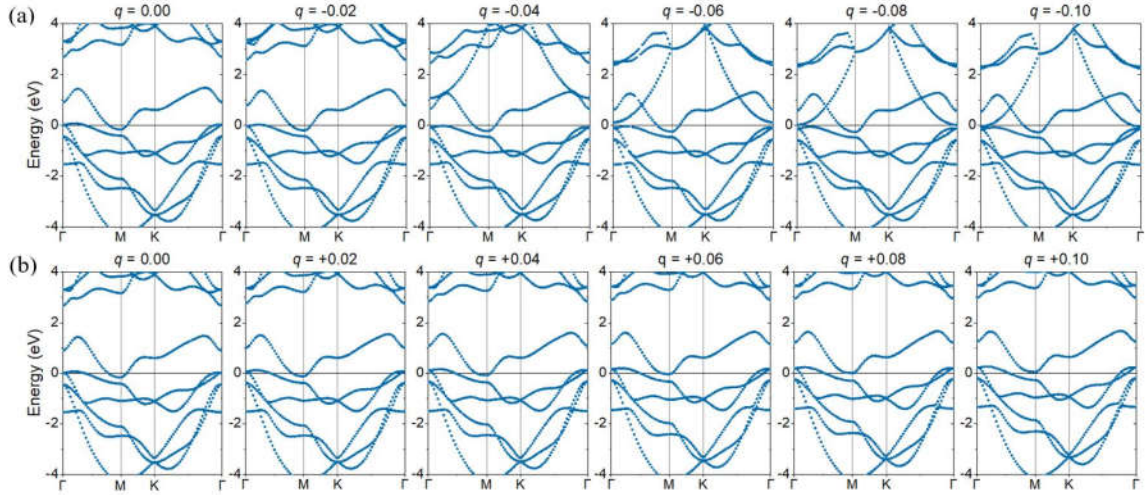

Fig. 3. Energy band structure of monolayer $SnTe_2$ with several (a) electron and (b) hole doping levels. The Fermi energies (dashed line) are set to zero for all plots.

To study the electronic properties of the monolayer SnX_2 under charge doping, we investigate the energy band structures of SnX_2 for the neutral ($q = 0$) and charge doping cases ($q \neq 0$). In Figs. 2 (a) and (b), we show the energy band structures of $SnSe_2$ under the electron and hole dopings, respectively. The dashed line shows the Fermi energy level. The obtained results show that $SnSe_2$ is a semiconductor with an indirect bandgap of 0.71 eV at the neutral case, which is in good agreement with the previous calculated result (0.8 eV) [30, 31]. We note that, the 1H-MoS_2 monolayer is direct-gap (1.65 eV) semiconductor [32], while the 1T-ZeS_2 monolayer is an indirect-gap (1.1eV) semiconductor [33]. For the electron doping case, the energy bands of monolayer $SnSe_2$ shift downward compared with the energy bands in the neutral case. Therefore, the monolayer $SnSe_2$ becomes metallic at the electron doping q = -0.04 e/atom. In the case of hole doping, the energy bands of $SnSe_2$ are almost unchanged by increasing q, as shown in Fig. 2 (b). On the other hand, the monolayer 1T-$SnTe_2$ is metallic at both neutral and charge doping cases, as shown in Figs. 3 (a) and (b). We can see that, for the electron doping, the energy bands of the monolayer $SnTe_2$ shift downward compared with the energy bands in the neutral case, while they are almost unchanged by increasing q for the hole doping case. With the stable metallic, 1T-$SnTe_2$ shows a potential for artificial muscle that

can work with a low applied voltage. Acerce et al. [12] showed that artificial muscle based on the metallic 1T- MoS_2 works with very low voltage ranging from -0.3V to 0.3V.

In Fig. 4, we show the actuator strain ε^q of the monolayer SnX_2 as a function of charge doping q ranging from -0.1 to +0.1 e/atom. In the neutral case (q = 0), we obtain ε^q =0. For the both electron and hole doping cases, ε^q of SnX_2 is non-linear function of q. For the electron doping case (q < 0), ε^q of the monolayer SnX_2 increases with decreasing of q. At q = -0.1 e/atom, the actuator strains of monolayer $SnSe_2$ is up to 1.8%, eight times higher than maximum strain (0.21%) for graphene-based actuator [11]. For the hole doping case (q > 0), $SnTe_2$ shows the highest compression strain (ε^q = -0.9%) at q = 0.06 e/atom, while $SnSe_2$ shows the highest compression strain (ε^q = -0.7%) at q = 0.05 e/atom and the expansion strain about (ε^q = 0.5%) at q = +0.1 e/atom.

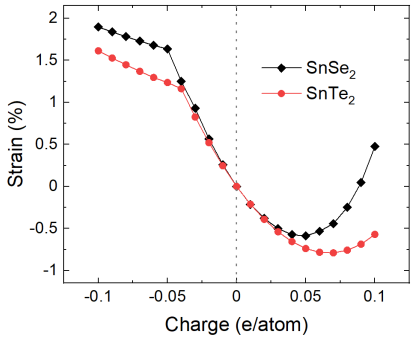

Fig. 4. Actuator strain of monolayer SnX_2 as a function of charge doping.

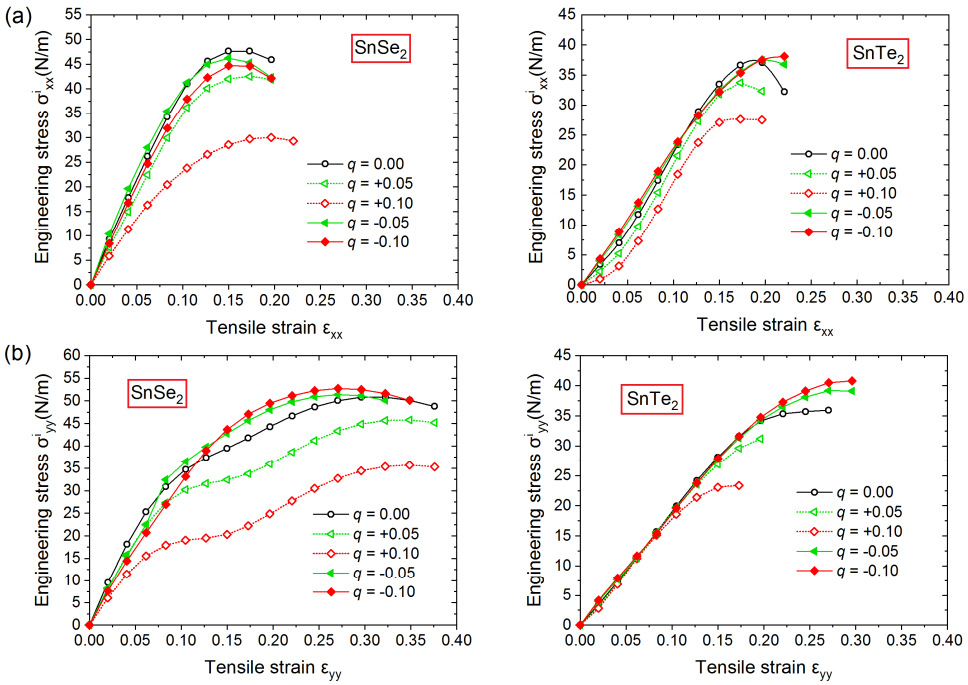

Fig. 5. Engineering stress of monolayer SnX_2 as a function of tensile strain for several charge dopings q. (a) σ_{xx} and (b) σ_{yy} along the x (armchair) and y (zigzag) directions of $SnSe_2$ and $SnTe_2$, respectively.

Finally, we investigate the ideal strength σ^i and the ideal strain ε^i of the monolayer SnX_2 under the tensile strain at different charge doping levels. In Figs. 5 (a) and (b), we show the stress-strain curves of $SnSe_2$ and $SnTe_2$ in the x (armchair) and y (zigzag) directions for several charge dopings, respectively. The obtained results indicate that SnX_2 shows an anisotropic behaviour with the tensile strain. We note that the strains along the armchair and zigzag directions can be applied to the 2D materials by controllably bending the substrate beam in a four-point apparatus [34]. At q = 0, σ^i

(ε^i) of $SnSe_2$ is 47.64 $N.m^{-1}$ (0.15) and 50.8 $N.m^{-1}$ (0.32) along the *x* and *y* directions, respectively. We note that although σ^i of $SnSe_2$ in the unit of $N.m^{-1}$ is larger than that of graphene ($\sigma^i \sim 37.87$ $N.m^{-1}$) [11], the thickness of $SnSe_2$ about 6.16 Å [35] is almost double the value of graphene (3.34 Å). Therefore, in the unit of GPa, σ^i_{xx} and σ^i_{yy} of $SnSe_2$ are 773 and 825 GPa, respectively, which are smaller than that of graphene (~ 1000 GPa). In addition, σ^i of $SnSe_2$ is higher than that of $SnTe_2$ for both *x* and *y* directions, as shown in Figs. 5 (a) and (b). For the hole doping ($q > 0$), the ideal stress is decreased by increasing $|q|$, in which highest reduction of σ^i is found in $SnSe_2$ along the armchair direction, as shown in Fig. 5 (a). In contrast, for the electron doping ($q < 0$), σ^i of $SnSe_2$ and $SnTe_2$ can increase by 3.8% and 13.4% in the zigzag direction, respectively, as shown in Fig. 5(b).

4. Conclusions

We have performed a first-principles calculations for the structural deformation and the electronic structure as a function of charge doping. Our results show that a semiconductor-metal transition occurs in the monolayer $SnSe_2$ for the electron doping at q = -0.04 e/atom. For the heavy electron doping, the actuator strain of $SnSe_2$ and $SnTe_2$ can be achieved up to 1.8% and 1.6%, respectively. Moreover, the ideal strength of $SnSe_2$ and $SnTe_2$ is increased by 3.8% and 13.4% for the zigzag direction in the case of electron doping, respectively. This study provides a guide for the design and fabrication of the monolayer SnX_2-based artificial muscles.

References

1. Mirvakili, S. M., Pazukha, A., Sikkema, W., Sinclair, C. W., Spinks, G. M., Baughman, R. H., & Madden, J. D. Niobium nanowire yarns and their application as artificial muscles. Advanced Functional Materials, 23(35), 4311-4316 (2013).
2. Mirvakili, S. M., & Hunter, I. W. Artificial muscles: Mechanisms, applications, and challenges. Advanced Materials, 30(6), 1704407 (2018).
3. Bar-Cohen, Y., Kim, K. J., Choi, H. R., & Madden, J. D. Electroactive polymer materials. Smart Materials and Structures, 16(2) (2007).
4. Ölander, A. An electrochemical investigation of solid cadmium-gold alloys. Journal of the American Chemical Society, 54(10), 3819-3833 (1932).
5. Carpi, F., & Smela, E. (Eds.). Biomedical applications of electroactive polymer actuators. John Wiley & Sons (2009).
6. Gallone, G., Carpi, F., De Rossi, D., Levita, G., & Marchetti, A. Dielectric constant enhancement in a silicone elastomer filled with lead magnesium niobate–lead titanate. Materials Science and Engineering: C, 27(1), 110-116 (2007).
7. Hung, N. T., Nugraha, A. R., & Saito, R. Charge-induced electrochemical actuation of armchair carbon nanotube bundles. Carbon, 118, 278-284 (2017).
8. Rogers, G. W., & Liu, J. Z. Graphene actuators: quantum-mechanical and electrostatic double-layer effects. Journal of the American Chemical Society, 133(28), 10858-10863 (2011).
9. Xie, X., Bai, H., Shi, G., & Qu, L. Load-tolerant, highly strain-responsive graphene sheets. Journal of Materials Chemistry, 21(7), 2057-2059 (2011).
10. Hung, N. T., Nugraha, A. R., & Saito, R. Two-dimensional MoS_2 electromechanical actuators. Journal of Physics D: Applied Physics, 51(7), 075306 (2018).
11. Van Thanh, V., & Hung, N. T. Charge-induced electromechanical actuation of two-dimensional hexagonal and pentagonal materials. Physical Chemistry Chemical Physics, 21(40), 22377-22384 (2019).
12. Acerce, M., Akdoğan, E. K., & Chhowalla, M. Metallic molybdenum disulfide nanosheet-based electrochemical actuators. Nature, 549(7672), 370-373. (2017)
13. Van Thanh, V., & Hung, N. T. Charge-induced electromechanical actuation of Mo-and W-dichalcogenide monolayers. RSC advances, 8(67), 38667-38672 (2018).

14. Zhou, X., Gan, L., Li, H., ... & Zhai, T. Ultrathin $SnSe_2$ Flakes Grown by Chemical Vapor Deposition for High Performance Photodetectors. Advanced Materials, 27(48), 8035-8041(2015).
15. Huang, Y., Xu, K., Wang, Z., Shifa, T. A., Wang, Q., Wang, F., ... & He, J. Designing the shape evolution of $SnSe_2$ nanosheets and their optoelectronic properties. Nanoscale, 7(41), 17375-17380 (2015).
16. Qu, L. H., Yu, J., Mu, Y. L.,... & Lu, T. S. Strain tunable structural, mechanical and electronic properties of monolayer tin dioxides and dichalcogenides SnX_2 (X= O, S, Se, Te). Materials Research Bulletin, 119, 110533 (2019).
17. Zeng, J., Liu, E., Fu, Y., Chen, Z., Pan, C., Wang, C., ... & Yan, X. Gate-induced interfacial superconductivity in 1T-$SnSe_2$. Nano letters, 18(2), 1410-1415 (2018).
18. Xiang, H., Xu, B., Xia, Y., Yin, J., & Liu, Z. Strain tunable magnetism in SnX_2 (X= S, Se) monolayers by hole doping. Scientific reports, 6(1), 1-8 (2016).
19. Giannozzi, P., Baroni, S., Bonini, N., Calandra, M., Car, R., Cavazzoni, C., ... & Dal Corso, A. QUANTUM ESPRESSO: a modular and open-source software project for quantum simulations of materials. Journal of physics: Condensed matter, 21(39), 395502 (2009).
20. Lejaeghere, K., Bihlmayer, G., Björkman, T., Blaha, P., Blügel, S., Blum, V., ... & De Gironcoli, S. Reproducibility in density functional theory calculations of solids. Science, 351, 6280 (2016).
21. Perdew, J. P., Burke, K., & Ernzerhof, M. Generalized gradient approximation made simple. Physical review letters, 77(18), 3865 (1996).
22. Monkhorst, H. J., & Pack, J. D. Special points for Brillouin-zone integrations. Physical review B, 13(12), 5188 (1976).
23. Broyden, C. G. The convergence of a class of double-rank minimization algorithms 1. general considerations. IMA Journal of Applied Mathematics, 6(1), 76-90 (1970).
24. Fletcher, R. A new approach to variable metric algorithms. The computer journal, 13(3), 317-322 (1970).
25. Goldfarb, D. A family of variable-metric methods derived by variational means. Mathematics of computation, 24 (109), 23-26 (1970).
26. Shanno, D. F. Conditioning of quasi-Newton methods for function minimization. Mathematics of computation, 24 (111), 647-656 (1970).
27. Li, G., Ding, G., & Gao, G. Thermoelectric properties of $SnSe_2$ monolayer. Journal of Physics: Condensed Matter, 29(1), 015001 (2016).
28. Sun, B. Z., Ma, Z., He, C., & Wu, K. Anisotropic thermoelectric properties of layered compounds in SnX_2 (X= S, Se): a promising thermoelectric material. Physical Chemistry Chemical Physics, 17(44), 29844-29853 (2015).
29. Qu, L. H., Yu, J., Mu, Y. L., Fu, X. L., Zhong, C. G., Min, Y., ... & Lu, T. S. Strain tunable structural, mechanical and electronic properties of monolayer tin dioxides and dichalcogenides SnX_2 (XO, S, Se, Te). Materials Research Bulletin, 119, 110533 (2019).
30. Cheng, Y. C., ... & Schwingenschlögl, U. Spin-orbit–induced spin splittings in polar transition metal dichalcogenide monolayers. EPL (Europhysics Letters), 102(5), 57001 (2013).
31. Lebègue, S., Björkman, T., Klintenberg, M., Nieminen, R. M., & Eriksson, O. Two-dimensional materials from data filtering and ab initio calculations. Physical Review X, 3(3), 031002 (2013).
32. Yue, Q., Kang, J., ... & Li, J. Mechanical and electronic properties of monolayer MoS_2 under elastic strain. Physics Letters A, 376(12-13), 1166-1170 (2012).
33. Lv, H. Y., Lu, ... & Sun, Y. P. Strain-induced enhancement in the thermoelectric performance of a ZrS_2 monolayer. Journal of Materials Chemistry C, 4(20), 4538-4545 (2016).
34. Conley, H. J., Wang, B., Ziegler, J. I., ... & Bolotin, K. I. Bandgap engineering of strained monolayer and bilayer MoS_2. Nano letters, 13(8), 3626-3630 (2013).
35. Tracy, B. D., Li, X., … & Smith, D. J., Characterization of structural defects in $SnSe_2$ thin films grown by molecular beam epitaxy on GaAs (111) B substrates. Journal of Crystal Growth, 435, 58-64 (2016).